

Inference on errors in industrial parts: Kriging and variogram versus geometrical product specifications standard

Giacomo Maculotti¹ | Giovanni Pistone² | Grazia Vicario³ 

¹Department of Management and Production Engineering, Politecnico di Torino, Turin, Italy

²de Castro Statistics, Collegio Carlo Alberto, Turin, Italy

³Department of Mathematical Sciences, Politecnico di Torino, Turin, Italy

Correspondence

Grazia Vicario, Department of Mathematical Sciences, Politecnico di Torino, Turin, Italy.
Email: grazia.vicario@polito.it

Abstract

This article focuses on the inference on the errors in manufactured parts controlled by using measurements devices. The characterization of the part surface topographies is core in several applications. A broad set of properties (tribological, optical, biological, mechanical, etc.) depends on the micro- and macrogeometry of the parts. Moreover, parts usually show typical deterministic geometric deviation pattern, referred to as manufacturing signatures, due to the specific manufacturing processes and process setup parameters adopted for their production. In several situations, the measurements may also be affected by systematic errors due to the measurement process, that might be caused, for example, by a poor part alignment during the measurement process. Measurement techniques and characterization methods have been standardized in the International Standard ISO 25178, defining parameters characterizing the surface topography and supplying methods and formula adapt to deal with this issue computationally. In the present article, we consider a type of spatial dependence between measured values at different points that suggest the use of the variogram to identify patterns in the parts. We offer a comparison, based on a real set of measures, between the latter approach and the conventional as a test of the efficient performance of our findings.

KEYWORDS

geometrical product specification, inspection strategies, Kriging, surface topography characterization, variogram

1 | INTRODUCTION

The surface topography of components draws its origin both by processing conditions and by process parameters.^{1,2} From a geometrical perspective and according to Leach,³ the surface topography (simply surface) of a component is its overall surface structure, consisting of the form (the underlying shape) and the texture, that is, what remains after removing the shape. Being intertwined with the manufacturing process, often the surface bears a systematic pattern which is unique and distinctive of the process: the so-named manufacturing signature.^{4,5} Experts estimate that 10% of component failures depend on an imperfect realization of topographical specifications.³ Consequently, measuring and characterizing the surface topography is core to understand and qualify manufacturing processes, to support the process optimization, and ultimately to enable the identification of deviations from the in-control state.

In the last few years, the industry has targeted the design of surface topography to engineer the functionality of products and increase their quality and performances. Topographies can control a wide range of functional properties,^{6,7} because most relevant physical phenomena, involving the exchange of energy and information, take place on the surfaces. Structured surfaces and texturing are relevant in several fields: biomedicine, where the microfluidics devices texturing aims to control and trigger the release of drugs in the patients based on physiological signals;⁸ robotics and manufacturing, which exploits texturing surfaces of handling components of robots to enhance the grip on objects to support the increasing human–machine interactions;⁹ automotive for achieving a significant reduction of both fuel consumption and pollutant emission by texturing engine components.^{10,11} Thus, the increasing demand for enhanced performances pulled fundamental research in electronics, energy, IT, optics, tribology, and other fields to enable surface functionalization.

All these applications require flexible and fast quality inspections relying on thorough, accurate and specific characterization methods, to meet customers demands, within the framework of Industry 4.0, and to deal with big data and interconnected cyberphysical systems.^{12–14} To this aim, surfaces measurement requires dense sampling through appropriate technology.¹⁵ Nowadays, new optical technologies are available to overcome the limitations of conventional inspection technologies based on contact probes (coordinate measuring machines, CMM) and contact stylus instruments.^{3,16} CMM may require too long times, hence high costs, to achieve an adequate sampling density. In some cases, the physical dimension of the probe forbids the measurement of statistically representative samples of the surface.^{16,17} Efficient surface modeling is a base requirement to cope with the challenges of surface characterization in the modern manufacturing of Industry 4.0,¹⁸ where free-form surfaces,¹⁹ additive manufacturing surfaces,^{20,21} and other nonstandard features appear.^{22–24} Different geometrical features, properties, and scales might be targeted depending on purposes and surface technology. In this article, the interest is focused on the height and width of features, in order to control the texture regularity, in terms of periodicities and isotropy.

Recently, literature has developed statistical modeling based on Kriging methods to aid inspection designers to overcome constraints and to enhance the informativeness of the measurement without increasing costs. In the following, we offer a review of this Kriging application.

1.1 | History

Pedone et al.²⁵ contains a first attempt to use Kriging modeling for the online design of inspection plans operated by CMM. The probing of a few point only leads to the assessment of nominal dimensions and shape, with benefits on the economy of the inspection process. The inspection plan as a sequential experiment to be designed online has shown the trade-off between accuracy and costs, exploiting an updating of the Kriging model iteratively, according to the new incoming data, and using the predictions from the updated model for selecting the next point to inspect. The article discussed two case studies about the verification of form tolerances, straightness, and roundness. Subsequently, Vicario et al.²⁶ have considered flatness tolerance verification, while Pistone and Vicario²⁷ discussed the improvement of wafer inspection strategies. Later on, Ruffa et al.²⁸ addressed the comparison between conventional and Kriging-based inspection strategies, from the perspective of measurement uncertainty. Ascione et al.²⁹ outlined adaptive inspection methods for coordinate measurement system based on Kriging modeling. Other authors have exploited the capability of Kriging models to detect geometrical and dimensional errors. Kolios et al.³⁰ developed predictive models for the reliability of cutting tools. Song et al.³¹ detect a geometrical deviation in additive manufacturing processes for polymers and Wang et al.³² outlined corrective models for this building strategy. Kriging models are of use also in the assembling to detect, and later correct, nonlinear assembling errors for compliant³³ and composite materials.³⁴

The Kriging modelization requires detecting and, consequently, modeling the correlation between measured responses. However, the choice of the most suitable class of correlation models, among the several available options, is not trivial. Several researchers, mostly geostatisticians, favor the use of the variogram, or semivariance diagram, in the choice of the correlation function. It is very informative about spatial dependence, showing the averaged square difference in the response values between a pair of measurement points separated by a given distance. Moreover, the variogram is equivalent to the correlation function for stationary processes, as frequently occurs (see Cressie³⁵).

This finding suggested further investigations on the relationship between variogram and correlation, see Pistone and Vicario.^{36,37} In the former case, the authors considered Gaussian vectors with constant variance. They showed how to parametrize the distribution with the variogram and, conversely, how to characterize all the Gaussian distribution with a given variogram. In the latter, they discuss the constraints imposed on the set of parameters defining the variogram.

Recently, Ruffa et al.³⁸ and Vicario et al.^{39,40} discussed the effectiveness of using variogram in other practical situations. Finally, a relevant article is Vicario and Pistone,⁴¹ whose main points provide the base the content of this article.

1.2 | State of art

Complex interactions between materials and manufacturing tools during the process can affect the surface texture, ultimately introducing manufacturing signatures. In most mechanical processes, such as machining or additive manufacturing, the process is repetitive and periodic. This situation results in a periodic texture and a spatial correlation between measured surface points. From here, the suggestion to use the variogram to investigate an existing surface topography correlation and infer geometrical properties of the surface. In Vicario and Pistone,⁴¹ the authors, exploiting simulative approaches, analyzed the variogram in the presence of both a noticeable trend in the model and anisotropy. If the manufacturing process is anisotropic, the variogram depends on both distances and direction. Contrary to some common beliefs, even for the most refined surfaces, the assumption of isotropy can fail. These features may show evidence of technological signatures or CMM systematic errors. The paper mentioned above represents a contribution to the adoptions of graphical tools in the quality control of the variability in spatial data.

Now in this article, the authors aim to prove that Kriging and variogram are adequate tools for quantitative characterization of surfaces. They provide a comparison with methods in the Standard, and theoretically support their findings in several practical case studies, one of which is presented in detail. Section 2 introduces the protocol recommended by the Standard for the characterization of the surface topography and the basic of Kriging. The use of Kriging prediction requires the computation of the weights assigned at measured points and this essential step depends on a suitable correlation model. Section 3 discusses variogram as an informative tool in fitting a model of spatial correlation. Section 4 provides the implementation of the two approaches of Section 2: a case study based on real measurements illustrates the methods, with a comparison of the respective performances. A final discussion concludes the article.

2 | SURFACE TOPOGRAPHY CHARACTERIZATION: STANDARD PROTOCOL AND KRIGING MODEL

2.1 | Standard characterization and protocol

A wide set of different technologies have been developed to enable surface topography measurements.^{15,16} Among the most widely used technologies for measuring surfaces, we mention contact probes (e.g., CMM and contact stylus instruments¹⁵), optical probes (point autofocus instruments^{42,43}), and surface topography optical instruments (like focus variation microscopes or coherence scanning interferometers¹⁵). They measure a cloud of points, resulting in a set of surface heights as a function $z(x, y)$ of plane coordinates (x, y) . The heights represent the departures of the measured topography from an arbitrary reference horizontal plane, usually the cartesian plane $z = 0$ representing the mean height.

Measurement techniques and characterization methods have been standardized in the ISO 25178.⁴⁴ Several areal height parameters and spatial parameters for describing, respectively, the statistical distribution of the surface height and the spatial orientation of the texture are on hand of the users. In the following, we provide a summary of the main, and most widely adopted, parameters and tools used to characterize surfaces according to the Standard ISO 25178-2:2012 protocol.⁴⁵

Among the most widely adopted height parameters, we mention the *arithmetic mean height* S_a and the *root mean square height* S_q , respectively,

$$S_a = \frac{1}{\text{meas}(A)} \iint_A |z(x, y)| \, dx \, dy,$$

and

$$S_q = \sqrt{\frac{1}{\text{meas}(A)} \iint_A z^2(x, y) \, dx \, dy},$$

where the definition domain A is the domain where the measured points are sampled and $\text{meas}(A) = \iint_A dx \, dy$.

It should be noted that the terms used in the ISO Standard sometimes differ from those used in Statistics. If $z(x, y)$ is the deviation from a reference value, and the normalized integral is intended as the expectation with respect to the uniform probability on A , then S_a is the absolute deviation,⁴⁶ and as such, it is a measure of the dispersion of the heights. This parameter is the metric used to quantify the roughness of the texture, which is relevant for tribological application, coupling tolerances and esthetic purposes.^{47,48} The parameter S_q is a standard deviation and is more informative than S_a both in terms of statistical meanings and physical relationship; in fact, it is linked to surface energy and optical properties.^{49,50} Since these two statistical moments cannot fully describe topographies, the knowledge of the surface height range is further required for sufficiently characterizing the amplitude of the height variability. To this aim, the *maximum height of the surface height* S_z is the most used parameter, to be used with caution since a drawback may be its sensitiveness to isolated and not significant peaks and pits.

Occasionally, the textures can exhibit imprints as anisotropy and/or periodicity, either due to a product functionalization or to manufacturing signatures. Detection and quantification of these defects are core for components functionality assessment and for process quality control. According to the Standard, the spatial parameters are the best suited for this analysis. They include the *autocorrelation function* f_{ACF} , the *autocorrelation length* S_{al} , the *texture aspect ratio* S_{tr} , and the *surface texture direction* S_{td} .

According to the ISO 25178-2:2012 the definition of f_{ACF} is

$$f_{ACF}(\tau_x, \tau_y) = \frac{\iint_A z(x, y)z(x - \tau_x, y - \tau_y) dx dy}{\iint_A z^2(x, y) dx dy}, \quad (1)$$

for all τ_x and τ_y such that $(x - \tau_x, y - \tau_y) \in A$ for some $(x, y) \in A$. Notice that, for each given (τ_x, τ_y) , the integration domain in the numerator is restricted to compatible (x, y) .

The other two parameters are defined by

$$S_{al} = \min\{\sqrt{\tau_x^2 + \tau_y^2} : f_{ACF}(\tau_x, \tau_y) \leq s\},$$

and

$$S_{tr} = \frac{p_{min}}{p_{max}},$$

where $p_{min} = S_{al}$ and $p_{max} = \max\{\sqrt{\tau_x^2 + \tau_y^2} : f_{ACF}(\tau_x, \tau_y) \leq s\}$.

The autocorrelation function is bounded between -1 and $+1$ and assumes the maximum value $+1$ at $\tau_x, \tau_y = 0$.

The autocorrelation length S_{al} is the horizontal distance of f_{ACF} which has the fastest decay to a specified value s , with $s \in [0, 1)$. The shape of f_{ACF} and the distance of decay below a threshold s can support the identification of periodic structures and of anisotropy. Opposite, if the spatial correlation is not a feature of the topography, it will decrease toward zero for increasing distances from the considered point. Moreover, the analysis of the autocorrelation decay in different directions can also identify the anisotropic pattern. Thus, S_{al} and S_{tr} , whose definition exploits the f_{ACF} , are designed to characterize the isotropy of the surface synthetically: the former measures the extent of the surface (auto)correlation, being the distance at which a portion of the surface is significantly different from the original location, and the latter quantifies the severity of the anisotropy. In fact, if the two correlation distances p_{min} and p_{max} are sufficiently similar, the surface can be considered isotropic, being S_{tr} the ratio between the smallest and largest distance of decay to s . Provided that $S_{tr} \in [0, 1]$, the surface is considered isotropic, if $S_{tr} > s$. The threshold s is conventionally⁵¹ set to 0.2 based on experts opinions on empirical practices without any formal rationale; clearly, the value of S_{al} and S_{tr} depends on the choice of s .

In the case of anisotropy, the direction of the anisotropy, that is, the main pattern, is orthogonal to the direction of S_{al} and is quantified, as an angle, by the *surface texture direction*, S_{td} , assessed from the Fourier spectrum of the surface, in polar coordinates, as the angle at which the spectrum has the maximum amplitude.

To this extent, the Fourier transform of $z(x, y)$ allows computing the spectrum of the surface heights, that is, the frequency-dependent amplitudes of $z(x, y)$, whose most typical representation makes use of the power spectrum density (PSD). The analysis of amplitude peaks of the spectrum enables the identification of the main harmonics, identifying the main frequency of the periodic pattern. Real surfaces typically show one of the main peaks at very low wavelengths: the

amplitude of this peak is related to the random variation of $z(x, y)$, according to signal theory.^{3,52} In general, adequate preprocessing is necessary to filter the wavelengths that are not relevant to the objectives of the characterization.

The ISO Standard characterization of a surface according to the mentioned parameters has been conceived to provide a quick, synthetic although conventional characterization. This approach has inherent limitations, mostly linked to the statistical robustness and the significance in the detection and the characterization of an existent anisotropy.

2.2 | Kriging

The concept of using Kriging methods in the research works mentioned in Section 1 to characterize surface topographies was prompted by their ability to make accurate predictions of a response basing on a limited set of spatial data and the reasonable assumptions that response values spatially close are much more alike than more distant values. This applies to Kriging methods as they consist in a spatial interpolation based on the correlation structure between the observations. In the following, Kriging methods are introduced in the essential parts, to outline their use in the comparison in Section 4. They rely on an optimality criterion that aims at minimizing the mean squared prediction error (MSPE) of the linear combination of observations, under the constraints of unbiasedness.

The ordinary Kriging model assumes that the observed values are realization of a Gaussian random field $Z(\mathbf{x})$ plus an unknown constant term β :

$$Y(\mathbf{x}) = \beta + Z(\mathbf{x}),$$

where $Z(\mathbf{x})$ denotes the value of the spatial field in the point $\mathbf{x} = (x_1, \dots, x_n)^T$ of the design space $\chi_q \subset \mathbb{R}^q$. In the case study in Section 4, $Z(\mathbf{x})$ is the height function introduced in the Section 2.1 ($q = 2$, $\mathbf{x} = (x, y)$) and its realizations are the measures obtained by measuring the surface points with respect to an horizontal reference plane at height β (usually $\beta = 0$). Moreover, the Gaussian random field is assumed to have zero mean and stationary covariance over the design space χ_q , that is, $\mathbb{E}(Z(\mathbf{x})) = 0$ and $\text{Cov}(Z(\mathbf{x}_i), Z(\mathbf{x}_j)) = \sigma_Z^2 R(\mathbf{h}; \boldsymbol{\theta})$, $i, j = 1, \dots, n$, where σ_Z^2 is the process variance and R is the spatial correlation function depending only on the displacement vector \mathbf{h} between any pair of points in χ_q and on a vector parameter $\boldsymbol{\theta}$. If the value of the autocovariance function $C(\mathbf{h})$ depends only on the length $\|\mathbf{h}\|$ of the vector \mathbf{h} , then the stochastic process is isotropic; opposite, the process is anisotropic. This property is vital in the characterization of the surface topography we deal with in Section 4.

Let now $\mathbf{Y}^n = (Y(\mathbf{x}_1), \dots, Y(\mathbf{x}_n))^T$ the vector of the observed values of the spatial field in the n sampled points \mathbf{x}_i , $i = 1, \dots, n$, and $Y_0 = Y(\mathbf{x}_0)$ the value in a new unsampled point \mathbf{x}_0 . The most popular prediction criterion is based on the minimization of the mean squared prediction error (MSPE), where the MSPE of $\hat{Y}_0 = \hat{Y}_0(\mathbf{Y}^n)$ is:

$$\text{MSPE}(\hat{Y}_0, F) = \mathbb{E}_F[(\hat{Y}_0 - Y_0)^2], \quad (2)$$

where F is the joint distribution of (Y_0, \mathbf{Y}^n) . The predictor in Equation (2) is unique, linear unbiased and the best one (BLUP) of $Y(\mathbf{x}_0)$. If the joint distribution F of (Y_0, \mathbf{Y}^n) is multivariate normal as in the ordinary Kriging, the MSPE in Equation (2) is equal to the conditional expectation of $Y(\mathbf{x}_0)$ given \mathbf{Y}^n :

$$\hat{Y}_0 = \beta + \mathbf{r}_0^T \mathbf{R}^{-1} (\mathbf{Y}^n - \beta \mathbf{1}) \quad (3)$$

with $\mathbf{1} = [1, 1, \dots, 1]^T$; \mathbf{R} is the correlation matrix with $r_{ij} = R(\mathbf{x}_i - \mathbf{x}_j)$ (i, j range from 1 to n), and $\mathbf{r}_0 = [R(\mathbf{x}_0 - \mathbf{x}_1), \dots, R(\mathbf{x}_0 - \mathbf{x}_n)]^T$ is the correlation vector. The predictor in Equation (3) minimizes the MSPE in Equation (2). Considering the interpolatory property of Kriging, MSPE is zero at the sampled points and it perfectly reflects the Kriging principle: it is large when \mathbf{x}_0 is away from the sampled points, small when it is close to them. Such a behavior expresses a measure of uncertainty of predictions, making possible to provide confidence intervals of the predictions.

It follows that:

$$\text{MSPE}(\hat{Y}_0) = \sigma_Z^2 (1 - \mathbf{r}_0^T \mathbf{R}^{-1} \mathbf{r}_0 + \mathbf{c}_0^T (\mathbf{1}_T \mathbf{R}^{-1} \mathbf{1})^{-1} \mathbf{c}_0^T) \quad (4)$$

with $\mathbf{c}_0^T = 1 - \mathbf{1}_T \mathbf{R}^{-1} \mathbf{r}_0$. The expression Equation (4) takes into account that β parameter is replaced by its generalized least squares estimator $\hat{\beta}$. Moreover, the unknown parameter vector $\boldsymbol{\theta}$ in $R(\mathbf{h}; \boldsymbol{\theta})$ can be estimated by maximum likelihood. It

has to be highlighted that Equation (4) underestimates prediction variance as it does not account for the extra variability transmitted to \mathbf{r}_0 , \mathbf{R} , and β by θ .

Concerning the correlation modeling in predicting the values of Y in unsampled points and in evaluating the MSPE in the predicted points, there are two approaches: the first one uses a spatial correlation function chosen within some parametric function families, driving this choice by some underlying phenomenon to model, choosing the parameter(s) in order to fit best the model;⁵³ the second approach, proposed by Matheron⁵⁴ exploits the variogram, defined as:

$$\gamma(\mathbf{x}_i, \mathbf{x}_j) = \frac{1}{2} \mathbb{E}((Z(\mathbf{x}_i) - Z(\mathbf{x}_j))^2).$$

Variogram may also be expressed in terms of the model covariance:³⁶

$$\gamma(\mathbf{x}_i, \mathbf{x}_j) = \text{Cov}(Z(\mathbf{x}_i), Z(\mathbf{x}_i)) + \text{Cov}(Z(\mathbf{x}_j), Z(\mathbf{x}_j)) - 2 \text{Cov}(Z(\mathbf{x}_i), Z(\mathbf{x}_j)).$$

Kriging method was originally intended as a model, to be used in Geostatistics, of the physical randomness of the quantity of interest. Later a different interpretation of the same method has been devised to treat Computer Experiments, where the traditional notion of randomness is not applicable.⁵⁵ In such a case, for each given covariance, the method produces an interpolation of the given values even if the covariance lack of any physical interpretation. The Kriging approach, within this framework, can thus be seen as a method to augment the density of sparse, that is, not densely sampled, measurement. The resulting surface can then be characterized according to the standard method.

The elicitation of a given covariance, together with the corresponding Gaussian distribution, corresponds then to the choice of a Bayes prior. Such a choice is made according to the qualitative type of the surface of interest. In this article, we follow this approach, with the addition of a special method for the choice of a covariance based on the use of variograms. The following Section 3 will be devoted to present and discuss in details the properties of the variogram.

3 | VARIOGRAMS

In this section, we present some facts about variograms and their estimation. We aim to illustrate how variograms can be used both to evaluate characteristics of the measured surface and to suggest a convenient covariance to be used for Kriging interpolation. The presentation is original in that it considers a definition that applies to both systematic and random sampling of the locations to be tested.

3.1 | Matheron's variogram

Let $Z = (Z(\mathbf{x}))_{\mathbf{x} \in A}$ be a real random field, where the set of locations A is endowed with a quasi-distance d . A quasi-distance is a symmetric relation that satisfies the triangle inequality. If, moreover, $d(\mathbf{x}, \mathbf{y}) = 0$ implies $\mathbf{x} = \mathbf{y}$, then d is a distance. In most applications we consider, A is either a planar connected graph, for example, a grid, or a plane real domain. In the first case, a distance could be a length on the graph. In the second case, the most common distance is $d(\mathbf{x}, \mathbf{y}) = \|\mathbf{x} - \mathbf{y}\|$ for some norm on 2-vectors.

Recall that the random field $(Z(\mathbf{x}))_{\mathbf{x} \in A}$ is *intrinsically stationary* if $\frac{1}{2} \mathbb{E}((Z(\mathbf{x}) - Z(\mathbf{y}))^2)$ depends only on the difference $\mathbf{h} = \mathbf{x} - \mathbf{y}$ through a *variogram function* γ , namely, $\mathbb{E}((Z(\mathbf{x}) - Z(\mathbf{y}))^2)/2 = \gamma(\|\mathbf{h}\|)$. If, moreover, the variogram function depends on $\|\mathbf{h}\|$ only, it is said to be *isotropic* (for that norm). See, for example, §2.2.1 of Cressie's monograph.³⁵ The previous definitions are inspired by the theory of stationary processes, where the stationarity is the invariance with respect to action of the translation group or of some other transformation group.

If both stationarity and isotropic intrinsic stationarity holds, with $\sigma^2 = \text{Var}(Z(\mathbf{x}))$, it is

$$\gamma(\|\mathbf{h}\|) = \frac{1}{2} \mathbb{E}((Z(\mathbf{x}) - Z(\mathbf{x} + \mathbf{h}))^2) = \sigma^2 - C(\mathbf{h}),$$

hence, the autocorrelation function $C(\mathbf{h})$ is a function of the norm. This variogram methodology is extensively used in Geostatistics and in Kriging modelization, see, for example, the monograph by Cressie.³⁵ In the original applications as discussed by Krige, and in many current applications, the variogram is assumed to be monotonic and bounded to

express the idea of a correlation fading out when the distance increases. *We do not make this assumption here.* For a deep mathematical discussion of variograms from the point of view of harmonic analysis see Sasvari⁵⁶ and Gneiting et al.,⁵⁷ while an exposition of the relevant mathematics of the Gaussian case can be found in Pistone and Vicario.³⁶

Now, we consider a variation of the standard setting, in that we assume, more generally, that the variogram depends on a quasi-distance d ,

$$\frac{1}{2}\mathbb{E}((Z(\mathbf{x}) - Z(\mathbf{y}))^2) = \gamma(d(\mathbf{x}, \mathbf{y})).$$

This assumption accommodates the instances where the points of A are identified by a nonnumeric label. In this case, we say that the process is *d-isotropic*.

The empirical estimator of the variogram studied by Matheron⁵⁴ is based on a *sampling plan* A_s , a finite subset of A . This estimator uses the values on A_s of a realization ω of the random mechanism to compute an estimate of γ at all possible nonzero values θ of the pseudo-distance on A_s , namely,

$$\tilde{\gamma}(\omega; \theta) = \frac{1}{2} \frac{1}{\#\{\mathbf{x}, \mathbf{y} \in A_s \mid d(\mathbf{x}, \mathbf{y}) = \theta\}} \sum_{\{\mathbf{x}, \mathbf{y} \in A_s \mid d(\mathbf{x}, \mathbf{y}) = \theta\}} |Z(\mathbf{x})(\omega) - Z(\mathbf{y})(\omega)|^2. \tag{5}$$

The Matheron estimator can be extended to all possible values of the distance by any interpolation or fitting method.

Clearly, as a random variable depending on the random sample ω , this estimator is unbiased and consistent under independent copies of the random field and a given fixed sampling plan. If the design is itself random, then unbiasedness and consistency will depend on proper assumptions on the device generating the sampling plan.

Another point of view is possible, that is, to consider the sample ω as fixed and the sampling plan random. This point of view is actually more adapted to the present setup. In fact, the measurement error is small if compared with the variability of the surface itself.

Let us discuss more in detail the argument above in order to derive an interesting generalization of the estimator of Equation (5). Given the sampling plan A_s , consider the set of all nondiagonal couples $\widetilde{A_s \times A_s} = \{(\mathbf{x}, \mathbf{y}) \in A_s \times A_s \mid \mathbf{x} \neq \mathbf{y}\}$. If the number of sampled points is $\#A_s = n$, then the number of nondiagonal couples is $n(n - 1)$.

For each fixed realization ω we have a couple of functions, both defined on $\widetilde{A_s \times A_s}$; namely we have the $n(n - 1) \times 2$ table

$\widetilde{A_s \times A_s}$	Γ	Δ
(\mathbf{x}, \mathbf{y})	$\frac{1}{2}(Z(\mathbf{x})(\omega) - Z(\mathbf{y})(\omega))^2$	$d(\mathbf{x}, \mathbf{y})$

and we look for a model to interpolate the column Γ as a function of the column Δ . The scatter plot of the table is called *variogram cloud* and any regression method could be used to produce an estimate of γ .^{35,41} The plot of the variogram cloud in a proper scale will provide us with a neat summary statistics of the data, see Figures 7 and 8.

The Matheron's solution is the computation of mean value for each distance value, that is, it is a conditional expectation. Namely, if we consider the uniform probability function on $\widetilde{A_s \times A_s}$, $s(\mathbf{x}, \mathbf{y}) = 1/n(n - 1)$, then

$$\tilde{\gamma}(\omega; \theta) = \frac{1}{2} \mathbb{E}_s(|Z(\mathbf{x})(\omega) - Z(\mathbf{y})(\omega)|^2 \mid d(\mathbf{x}, \mathbf{y}) = \theta).$$

The conditional expectation above defined for each realization of the original random field model depends on the sampling plan only.

The idea to consider generic sampling measure originally arose in the discussion of the application of the Kriging methodology to random fields of the form $(F(\mathbf{x}) + Z(\mathbf{x}))_{\mathbf{x} \in D}$, where $(Z(\mathbf{x}))_{\mathbf{x} \in D}$ is intrinsically stationary and F is a deterministic function.⁴¹ If the deterministic part F is prevalent to the random part Z , then the Matheron variogram tells more about the features of F than about the correlation structure of Z . The effects of the deterministic trend and the correlation are confounded in the variogram and could be difficult to evaluate which one prevails, by inspection. Nonetheless, the tool is useful in two ways. If the deterministic effect is assumed to be prevalent, a proper model, suggested by the shape of the variogram, can be introduced in the Kriging model via a term $\beta(\mathbf{x})$ in order to compute residuals representing the $Z(\mathbf{x})$ term. Or, in the other case, the variogram can be used to evaluate the correlation in a Kriging model with constant β .

In the following section, we discuss the first case, and we show how to define the variogram of a deterministic function F . This plan requires a generalization of the Matheron estimator in a way that ignores (provisionally) the effect by the random field and focusses on the randomness that comes from the sampling design.

3.2 | Empirical variogram or G-variogram

This section is a review of the properties of the variogram redefined as follows.

Definition 1. Let A be a domain endowed with a semidistance d and ν a symmetric probability measure on $A \times A$. Given a bounded response function of interest $F : A \rightarrow \mathbb{R}$ and $(X, Y) \sim \nu$, the empirical variogram, or G-variogram, of F with respect to ν is a regular version γ_F of the conditional expectation of $\frac{1}{2}(F(X) - F(Y))^2$ given $d(X, Y)$, that is,

$$\mathbb{E}_\nu \left(\frac{1}{2}(F(X) - F(Y))^2 | d(X, Y) \right) = \gamma_F(d(X, Y)).$$

In the definition above, the joint distribution ν is intended to give a theoretical model of the sampling plan. The simplest case is independent sampling as it is the case in Matheron estimator.

Expansion of the square gives

$$\gamma_F(d(X, Y)) = \frac{1}{2}\mathbb{E}_\nu(F(X)|d(X, Y)) + \frac{1}{2}\mathbb{E}_\nu(F(Y)|d(X, Y)) - \mathbb{E}_\nu(F(X)F(Y)|d(X, Y)),$$

where the two first terms in the right-hand side are equal because ν is symmetric. Notice that the last term, without the minus sign, is similar to the autocorrelation function (1) when the sampling measure is uniform on the set $\{\mathbf{x}, \mathbf{x} + \boldsymbol{\tau}\}$.

The G-variogram function is defined only on the support of the semidistance d under the distribution ν . By polarization, a bilinear nonnegative definite joint G-variogram $\gamma_{G,F}$ can be defined. Instead, the definiteness of the G-variogram function could be considered only in particular cases, precisely when the set of possible distances is a semigroup.

We conclude this discussion by observing that the use of a quasi-distance appears in applications where the directional G-variogram is the index of interest.⁴¹ For example, $d((x_1, y_2), (x_2, y_2)) = |x_1 - x_2|$ allows to bring to light variations in one direction, here the first coordinate direction. This case is of high practical interest as when anisotropy occurs. Both the toy examples and the case study below present an instance of such a feature.

3.3 | General properties of the variogram

Here is a list of simple general properties of the G-variogram that show how the features of F affect γ_F .

1. The effect of an affine transformation is, see p. 72 of Cressie,³⁵

$$\gamma_{\alpha F + \beta} = \alpha^2 \gamma_F.$$

2. If the sampling joint distribution is symmetric, $(X, Y) \sim (Y, X)$, we have

$$\begin{aligned} \gamma(d(X, Y)) &= \frac{1}{2}\mathbb{E}(F(X)^2 | d(X, Y)) + \frac{1}{2}\mathbb{E}(F(Y)^2 | d(X, Y)) - \mathbb{E}(F(X)F(Y) | d(X, Y)) \\ &= \mathbb{E}(F(X)^2 | d(X, Y)) - \mathbb{E}(F(X)F(Y) | d(X, Y)). \end{aligned}$$

Notice the similarity with the stationary random field case. In particular, assuming independence,

$$\mathbb{E}(\gamma(d(X, Y))) = \mathbb{E}((F(X) - F(Y))^2) = \text{Var}(F(X)).$$

3. The maximal variation of F at comparable distances is an important feature of the response function. Precisely, if F is d -Lipschitz, that is,

$$|F(x) - F(y)| \leq \|F\|_{\text{Lip}} d(x, y)$$

and $\|F\|_{\text{Lip}} = \min_{x \neq y} |F(x) - F(y)|/d(x, y)$, then

$$\begin{aligned} \gamma(d(X, Y)) &= \frac{1}{2} \mathbb{E}(|F(X) - F(Y)|^2 |d(X, Y)) \\ &\leq \frac{1}{2} \mathbb{E}(\|F\|_{\text{Lip}}^2 d(x, y)^2 |d(X, Y)) = \frac{\|F\|_{\text{Lip}}^2}{2} d(x, y)^2, \end{aligned}$$

that is, the graph of γ as a function of the distance $t = d(x, y)$ is bounded by a parabola, $\gamma(t) \leq \frac{1}{2} \|F\|_{\text{Lip}}^2 t^2$.

4. In general, the *interaction variogram* can be defined by

$$\mathbb{E}((F_1(X_1) - F_1(X_2))(F_2(X_1) - F_2(X_2)) |d(X_1, X_2)) = \gamma_{1,2}(d(X_1, X_2)),$$

so that, with obvious notations,

$$\gamma_{1+2}(t) = \gamma_1(t) + \gamma_2(t) + \gamma_{1,2}(t).$$

In order to appreciate the potential interest of the methodology, we discuss some toy examples below. Note that we will plot the variograms in the scale $\sqrt{2\gamma}$. In fact, the Lipschitz inequality computation above suggests plotting in a scale which is linear in the distance.

3.4 | 1d examples

Let us consider the simple case, where, with no restriction of generality, the metric space is the unit interval, $A =]0, 1[$, endowed with the standard distance $d(x, y) = |x - y|$. Assume the sampling random variables X and Y are IID with uniform common distribution on A .

The distribution of the conditioning random variable $d(X, Y) = |X - Y|$ has a triangular density $t(\rho) = 2(1 - \rho)$ if $0 < \rho < 1$, and $t(\rho) = 0$ otherwise.

The variogram γ is characterized by the master equation

$$\begin{aligned} &\int_0^1 \int_0^1 \frac{1}{2} |F(x) - F(y)|^2 \Phi(|x - y|) \, dx dy \\ &= \int_0^1 \int_0^1 \gamma(|x - y|) \Phi(|x - y|) \, dx dy = \int_0^1 \gamma(\rho) \Phi(\rho) t(\rho) d\rho, \end{aligned}$$

where the last integral is the result of the change of variable $\rho = |x - y|$ and Φ is any measurable function such that the integral exists. Because of the symmetry, the first integral is

$$\begin{aligned} &\int_{0 < x < y < 1} |F(x) - F(y)|^2 \Phi(y - x) \, dx dy \\ &= \int_0^1 \left(\frac{1}{2(1 - \rho)} \int_0^{1-u} |F(v) - F(\rho + v)|^2 \, dv \right) \Phi(\rho) t(\rho) \, d\rho, \end{aligned}$$

where $u = x - y$ and $v = x$.

In conclusion, the variogram is

$$\gamma(\rho) = \frac{1}{2(1 - \rho)} \int_0^{1-\rho} |F(v) - F(\rho + v)|^2 \, dv. \quad (6)$$

Let us consider a few typical cases, illustrated in Figures 1 and 2. All the graphs in this section are done with the Wolfram Mathematica suite.

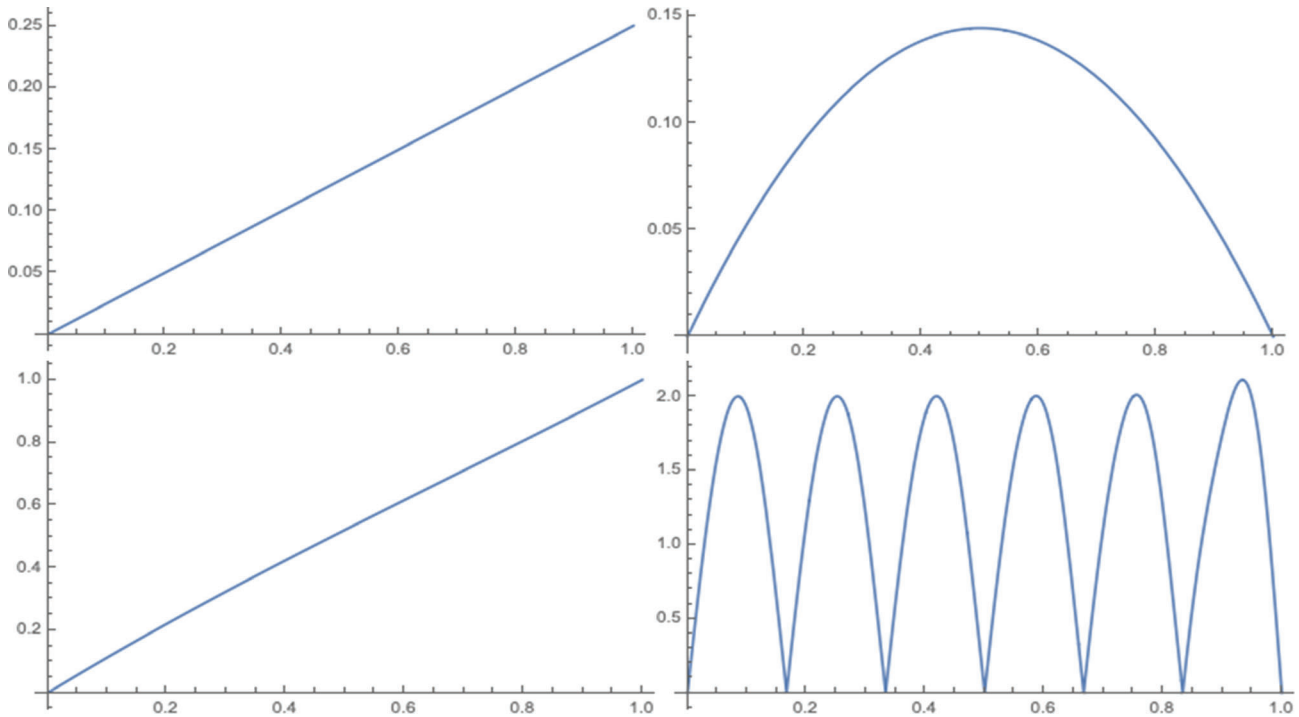


FIGURE 1 Examples of G-variograms γ_F . The four cases show how the shape of F is reflected in the shape of γ_F . The cases of F are, left to right, top to bottom: Affine function $F(x) = 1 + \frac{1}{4}x$; parabolic bump $F(x) = x(1 - x)$; parabolic bend $F(x) = 1 - x^2$; sine function $F(x) = \sin(6(2\pi)x)$

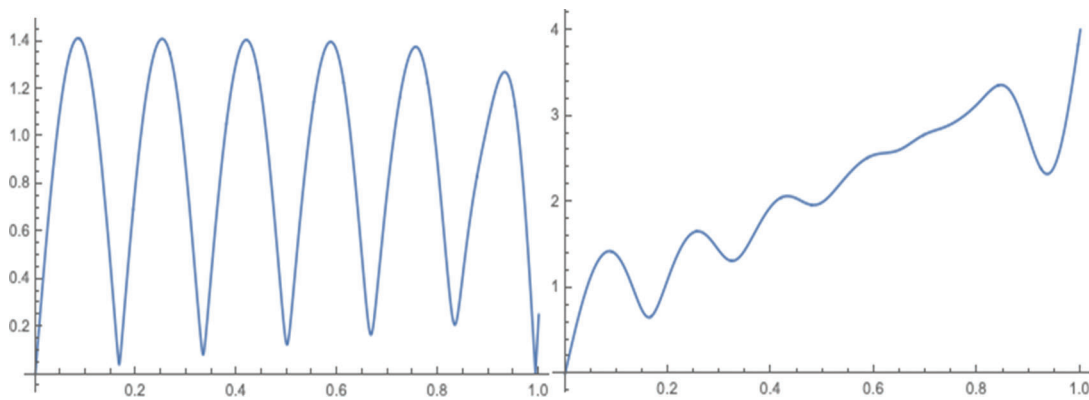


FIGURE 2 Examples G-variogram showing the effect of the superpositions of a linear and a sinusoidal shape: $F(x) = \frac{1}{4}x + \sin(6(2\pi)x)$ (left) and $F(x) = 4x + \sin(6(2\pi)x)$ (right)

Affine F

If F is affine, $F(x) = ax + b$, then

$$\gamma(\rho) = \frac{1}{2(1 - \rho)} \int_0^{1-\rho} a^2 \rho^2 dv = \frac{1}{2} a^2 \rho^2.$$

This example clearly supports the choice to plot $\sqrt{2\gamma}$ instead of γ itself.

A bound on F

If $|F| \leq k$, then $\frac{1}{2}|F(x) - F(y)|^2 \leq 2k^2$. If F is Lipschitz, $|F(x) - F(y)| \leq a|x - y|$, then $\gamma(\rho) \leq \frac{1}{2}a^2\rho^2$, see Item (3) in the list of properties above. If moreover $F(0) = 0$, then $F \leq |a|$, and the bound is $\min(a^2\rho^2, a^2) = a^2\rho^2$.

Bended F

Consider $F(x) = 4hx(1-x)$ or $F(x) = 1-x^2$. In such cases, the computation and the qualitative analysis are both simple. See Figure 1

Periodic F

Let us consider a periodic function, $F(x) = \sin(k(2\pi)x)$. In this case,

$$(F(v) - F(u+v))^2 = \left(\sin\left(\frac{2\pi}{k}v\right) - \sin\left(\frac{2\pi}{k}(u+v)\right) \right)^2 \\ \left(\sin\left(\frac{2\pi}{k}v\right) - \sin\left(\frac{2\pi}{k}u\right) \cos\left(\frac{2\pi}{k}v\right) + \sin\left(\frac{2\pi}{k}v\right) \cos\left(\frac{2\pi}{k}u\right) \right)^2.$$

Superposition

Let us consider the case of superposed functions. The variogram of $F_1 + F_2$ appears to be difficult to understand in terms of the separate variograms because there is an interaction term:

$$\gamma_{1+2} = \gamma_1 + \gamma_2 + \gamma_{1,2},$$

where $\gamma_{1,2}$ is defined by the polarized version of the definition of γ . Figure 2 provides two examples of superposed affine and periodic shapes with different relative weights.

3.5 | Discussion of the examples

Let us review the purpose of the exercises above. The idea is to motivate the use of variograms with sampled points in the characterization of surfaces. Consider a response surface on a given real domain A (usually a rectangle). A measurement is available at each testing points $\mathbf{x} \in A$. We want to assess the conformity of the shape of the response surface to some standard. For example: “is the surface bended in some direction?” Or: “Is there a waviness of a type associate to a specific technology?” These are possible defects that cannot be specified in a parametric way.³⁹

A very popular modeling method relies on the assumption that the surface under study is the realization of a random field, for example, a Gaussian random field $(Z(\mathbf{x}))_{\mathbf{x} \in A}$. In such a case, the observed characteristics of the surface will, in fact, depend on the autocovariance of the random field.

Even if the surface under examination is not random in any physical sense, the examples show that one can use the G-variogram to assess some specific features, such as the waviness.

Moreover, one can perform the prediction of the response at untried points by a Bayesian Kriging interpolation based on the elicitation of a covariance. In this case, the form of the variogram will suggest the choice of a reasonable and compatible covariance.³⁵ That is, knowledge about the variogram provides knowledge about the correlation and, in turn, a least square prediction of the response at untried points.^{27,36,54} We stress that this methodology is not a method of estimation of a correlation, but it is a method of elicitation of a Gaussian prior, as it is illustrated in the following section. In fact, the empirical variogram is not a bona fide variogram, that is, it does not necessarily satisfy the negative-definite condition. For this reason, the associated autocovariance could be negative definite. See, for example, the discussion in Gneiting et al.⁵⁷ and Stehlik et al.⁵⁸ Concerning the latter paper, the authors proved that the probability of choosing a negative-definite covariance when dealing with empirical financial data is high. The same issue might happen when a sequential design is used in the measurement process, mainly when ad hoc software are blindly used to overcome computational features. Therefore, possible topics to be investigated are the next-point selection criteria that may look for geometric variograms corresponding to positive-definite covariance structure.

4 | CASE STUDY

This section presents a case study to show the effectiveness and the potential of the methodologies formerly discussed. A real surface has been densely measured by an areal surface topography measuring instrument, achieving a very large

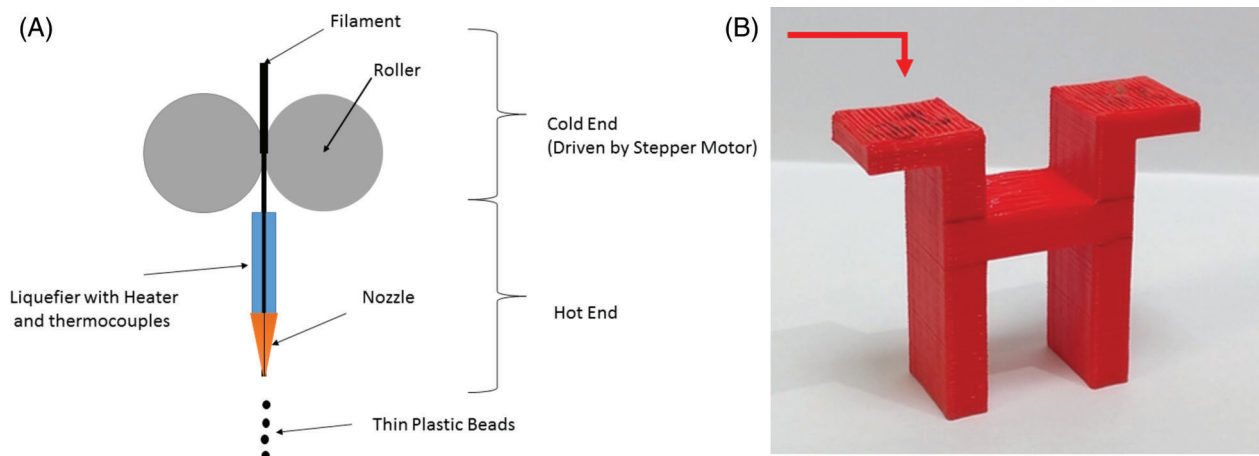


FIGURE 3 (A) Schematic of FDM process and (B) manufactured specimen. The top left surface, indicated by the arrow, has been characterized

set of data (10^6 measured points) and the characterization of surface topography has been carried out according to the Standard protocol, as presented in Section 2.1. Then, considering only a very small subset (0.4%) of the measured data, a larger number of the surface points has been predicted using Kriging and variogram. The set of the predicted points was used for characterizing the surface according to the standard protocol. The comparison between the parameters obtained according the two ways of approaching the problem is in favor of Kriging and suggests final considerations.

The standard characterization method is applied through the commercial software Mountains Map 7.4.

4.1 | Materials and methods

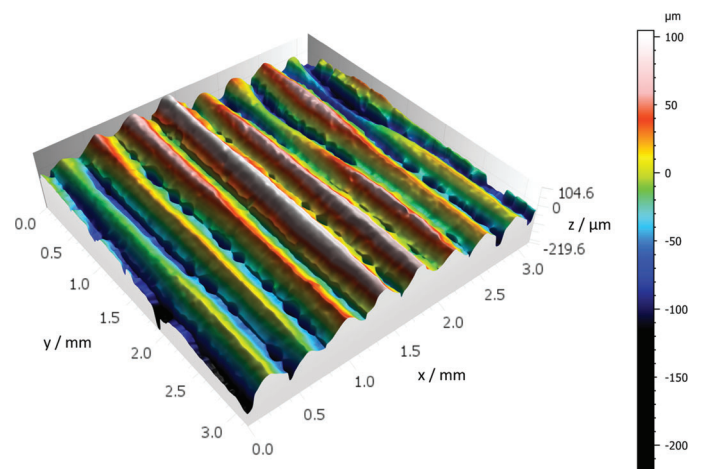
Modern industry, within the paradigm of Industry 4.0, experiences a constant increase in the demand for flexibility and customization of products.¹⁸ This has led to the development of innovative manufacturing strategies in the production processes to satisfy customer requirements. Additive manufacturing (AM) outstands other solutions for its capability to optimize the design of components and the material and energy consumption.⁵⁹ Due to its flexibility in a wide range of application, we focus on the fused deposition modeling (FDM), that is, an additive process for polymeric material. The component is manufactured by fusing a wire of material, deposited layer-by-layer raster scanning the layer cross-section of the part. Figure 3(A) represents a schematic view of the process; Figure 3(B) shows the manufactured specimen with a benchmark geometry.

The top surface topography of the specimen (indicated by a red arrow) has been measured exploiting an area surface topography measuring instrument (Figure 4): coherence scanning interferometer (CSI), a Zygo NewView 9000 equipped with a 20 \times objective and a 0.5 \times digital zoom. This instrument provides a high measurement speed, and is a state of the art instrument for the inspection of topographies. Thanks to the measurements acquisition capability of the CSI instrument, a dense sampling of the surface, with a lateral resolution of 3.56 μm , was made possible, resulting in one million measured points.

4.2 | Results

4.2.1 | CSI measurements

The surface topography based on the measured points is shown in Figure 5, where the manufacturing signature is clearly noticeable as a waviness pattern along the x -axis; also a deviation from planarity can be highlighted, even though at a minor extent. The measured topography is consistent with the known manufacturing signature of the FDM process, due to the raster scanning approach according to which the layers are built; in fact, the signature unfolds in a periodic pattern resembling the adjacent deposition of the molten wires of material. Given the high density of the measured points, the representation of the surface topography in Figure 5 may be considered faithful to the real one. Therefore, the comparison

FIGURE 4 The CSI Zygo NewView 9000**FIGURE 5** 3D plot of the surface topography $z(x,y)$ measured by the CSI. It may be considered a faithful representation of the real surface topography

we perform considers that surface as the real one and the CSI measurements as the reference to qualify the effectiveness of the Kriging method in predicting surface topographies.

To this aim, the main parameters (according to Standard, see Section 2) for the characterization of the surface texture are computed, using the large data set of CSI measurements and by means of the commercial software Mountains Map v7.4. As the object of the characterization is the surface texture, the waviness surface, that is, the S-F surface,⁴⁵ is considered¹. The resulting surface texture parameters are in Table 1 and the corresponding PSD is represented in Figure 6. The first three parameters, S_a , S_q , and S_z , characterize the surface heights, highlighting hills and valleys with respect to

¹The operators sequence involve an S-operator (i.e., a high-pass filter) with cut-off of 80 μm , and an F-operator for leveling.

Parameter	S_a (μm)	S_q (μm)	S_z (μm)	S_{al} (mm)	S_{tr}	S_{td}
Value	36.1	45.5	326	0.149	9.5%	178.0°

TABLE 1 Surface texture parameters according to ISO 25178-2:2010, computed on CSI measurement data and by means of the dedicated software MountainsMap

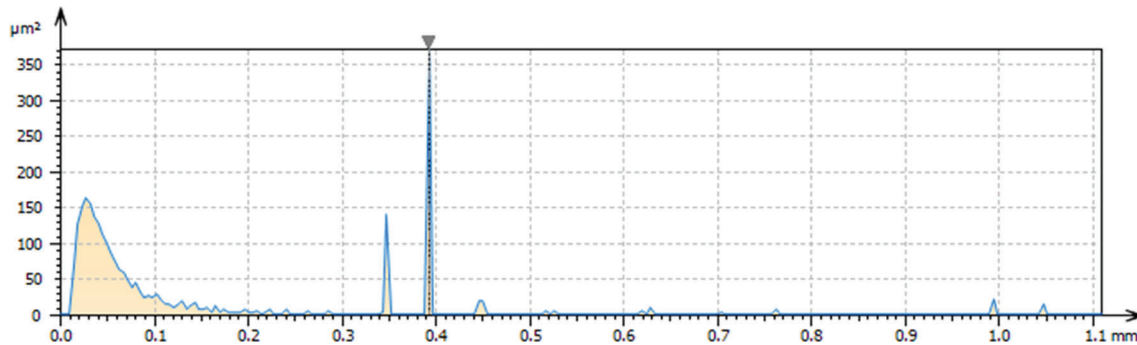


FIGURE 6 Power spectrum density of the surface topography according to CSI measurements

the reference cartesian coordinate plane, set at the average height, $z = 0$. The other three parameters, S_{al} , S_{tr} , and S_{td} , are for the detection of possible anisotropies. The anisotropy of the surface is highlighted according to the standard analysis through the isotropy parameter S_{tr} , that relies on the evaluation of S_{al} . S_{tr} is 9.5%, definitely less than the conventional threshold of 20%, and the texture pattern direction, which describes the direction of the anisotropy measured by the parameter S_{td} , is at 178° (or equivalently at -2°) with respect to the x -axis. As regards the analysis of the PSD graph, computed as the average of the PSD evaluated in all possible directions, it can be noticed the main harmonic, that is, the base wavelength, at 0.39 mm. The recognized wavelength is coherent with the surface topography in Figure 5, pointing out the manufacturing signature and its entity. There is a second relevant harmonic in close proximity of zero (at 0.027 mm): this feature represents the noise content of the surface, due to measurement noise and local random variability of the surface.

4.2.2 | Variogram and Kriging prediction

Since we aim at proving the adequateness of Kriging methodology in increasing the measurement informativeness of slow and low-resolution surface measurement instruments (as CMMs and contact styluses), a sample from the dense surface set of points measured using the CSI was randomly extracted to be used as input of the Kriging prediction model. The sample size was 4000 points, only the 0.4% of the 10^6 measured points; this size is meant both to be representative of the low-resolution measurement system, simulating a sparse measurement, and to make the comparison more persuasive. In fact, this scenario may also happen in situations in which, after a process optimization requiring thorough expensive characterization (e.g., based on optical surface topography instruments) and yield reference information about the surface, subsequent cheaper online quality controls may be performed using less expensive but slower instruments. The choice of the random sampling is aimed at enabling inferences on the statistical distribution and properties of the results.

As the first step, the empirical variogram (as suggested in Section 3.1) was computed. In Figure 7, the variogram cloud and the (omni-directional) variogram, based on the Euclidean distance and according to the Matheron's estimator, are represented.

The variogram exhibits a structured correlation; the behavior due to the sampled points significantly and systematically differs from that of a set of points measured on a planar surface, without any systematic behavior. In particular, two deviations from planarity can be appreciated: a periodic pattern superimposed to a polynomial trend (second-order seems suited). Such behavior suggests the presence of a sinusoidal texture and of a systematic deviation from planarity that can be generally described by a polynomial of at least first order (recall that a quadratic variogram characterizes a linear relationship between responses). The variograms along the x - and y -axis have been evaluated, to investigate the possible presence of anisotropy. These directions have been chosen knowing the technological characteristics of the process, which introduces periodicities and structured correlations only in orthogonal directions. A pronounced waviness, see Figure 8(A), is highlighted by the variogram along the x -axis, whereas the variogram along the y -axis in Figure 8(B) does

FIGURE 7 Omni-directional variogram cloud and estimated variogram (in red), that suggests the presence of a structured correlation. Its directionality is investigated in Figure 8

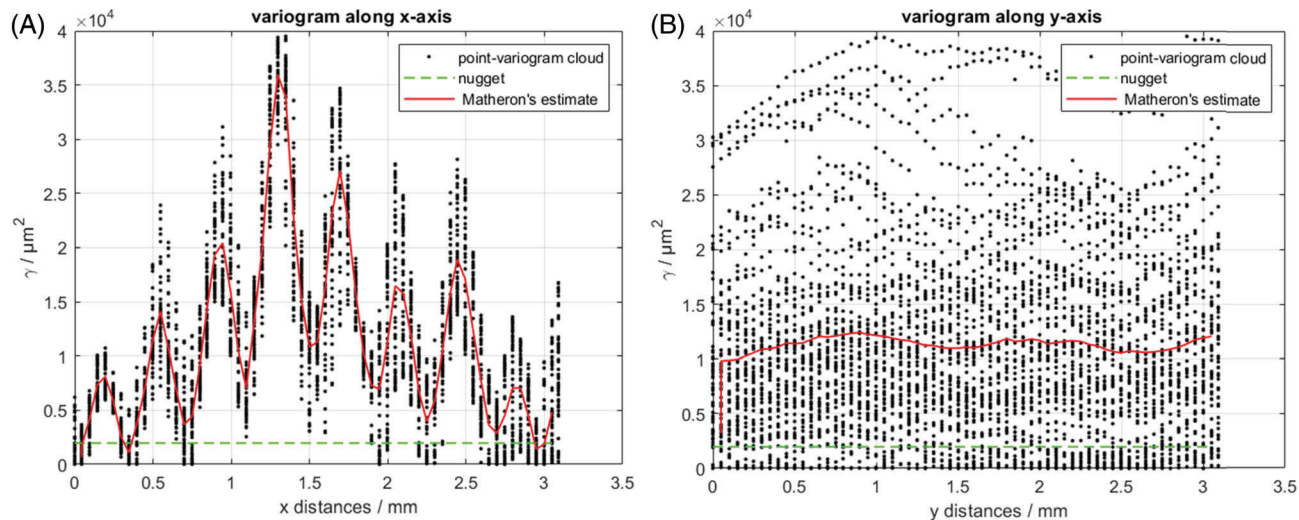
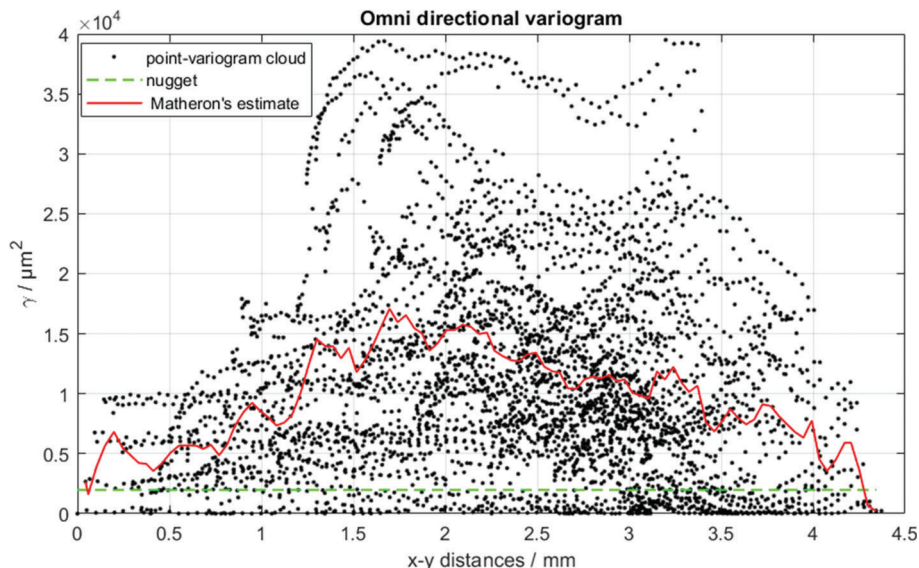


FIGURE 8 Variogram clouds along the (A) x-axis and (B) y-axis. In red the correspondent empirical variograms

not reveal a departure from the planarity of the surface and there is no evidence of any correlation structure. Therefore, the two one-directional variograms detect severe anisotropy.

Relying on these findings, the height of the surface was predicted at 62,500 points (representing the 6.25% of the measured points data set). It should be noted that computational constraints limited the size of the Kriging prediction set; but it is not so small if compared with the starting data set (4000 points), resulting in about 6.4% the percentage of predictor points to predicted ones.

Kriging predictions have been computed exploiting the DACE toolbox of MatLab 2019b, and relying on a supervised procedure to choose the functional form of the spatial correlation function. Provided the knowledge of the variogram, a cubic spline function has been selected, because, among the available ones in the toolbox, it is the aptest to model a wavy trend. The spatial correlation along the y-axis was a constant and the overall correlation results from the product of the two.³⁸ The toolbox, to achieve the Kriging prediction, recomputed the spatial correlation based on the sampled points; the model caters for anisotropy by differently choosing the spatial correlation function parameters for the two spatial directions.

The surface topography, obtained with Kriging predictions of the heights, is represented in Figure 9. The manufacturing signature due to waviness can still be appreciated along the x-axis direction, despite the poor sampling density. The

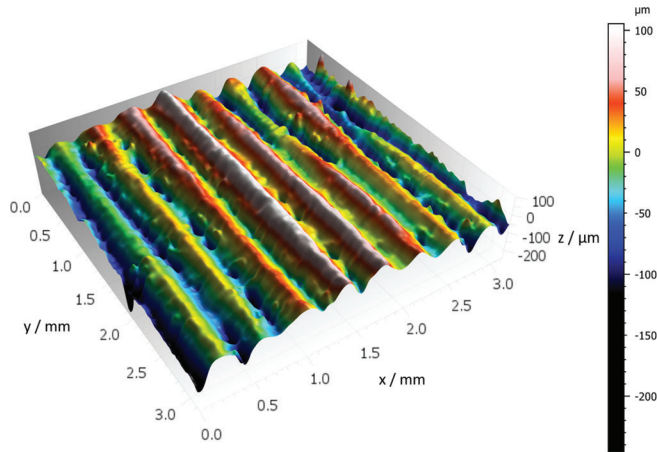


FIGURE 9 3D plot of the surface topography $z(x,y)$ obtained through the application of Kriging. This results has to be compared with Figure 5

Parameter	S_a (μm)	S_q (μm)	S_z (μm)	S_{al} (mm)	S_{tr}	S_{td}
Value	35.6	44.8	325.5	0.152	10.3%	180.0°

TABLE 2 Surface texture parameters, of the Kriging-interpolated surface, computed according to ISO 25178-2:2010 by means of the dedicated software MountainsMap

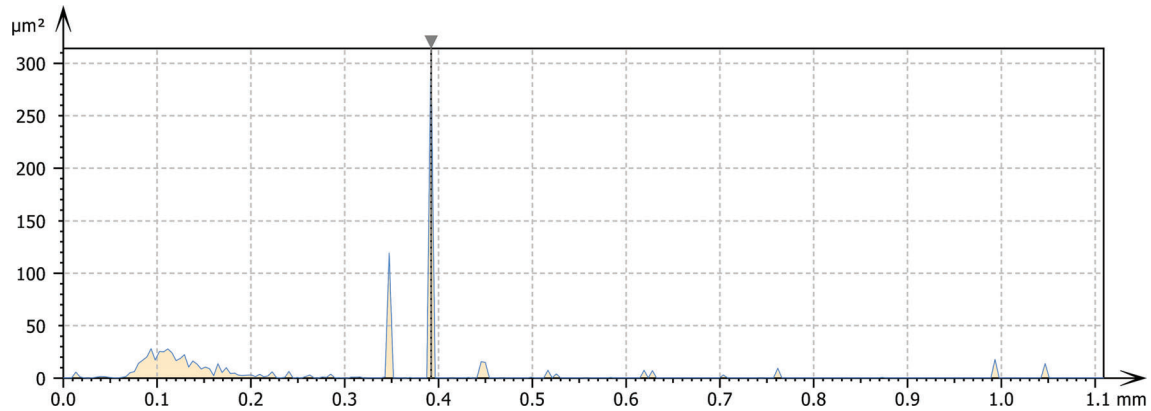


FIGURE 10 Power spectrum density of the Kriging-interpolated surface

predicted surface has been characterized, considering its points as measured ones, to provide a quantitative comparison: the surface texture parameters (summarized in Table 2) and the PDS (shown in Figure 10), according to the Standard, have been computed.

Comparing the results in Table 1, based on 10^6 measured point with the CSI, with the results in Table 2, computed on the predictions based on 0.4% of the mentioned measured points, it can be stated that the surface is still correctly characterized as anisotropic with the parameter S_{tr} significantly smaller than 20% and the texture pattern is directed at 178.7° (i.e., -1.3°) with respect to the x -axis. The main harmonic representing the base wavelength is evaluated correctly at 0.39 mm. Due to the interpolation inherent in the Kriging, very low scale variation can be only partially captured. In fact, the PSD of the interpolated surface shows a peak at 0.1 mm (see Figure 10). This harmonic is near the upper bound of the noise frequency of the CSI measured surface (0.027 mm) and shows that the procedure based on the Kriging acted as a high-pass filter.

A possible way to investigate the nature of the slight differences between the surface topography parameters in Tables 1 and 2 can be sought in the analysis of the interpolation error, shown in Figure 11. Not particular trends can be highlighted, and larger errors are at the edges of the investigated domain, which is typical for interpolation methods.^{55,60} Moreover, considering the spectral content of this interpolation error, shown in Figure 12, only one harmonic at 0.021 mm can be noticed, which is not far from the noise content of the original data set, that is, 0.027 mm.

FIGURE 11 Surface topography of interpolation error of the Kriging prediction

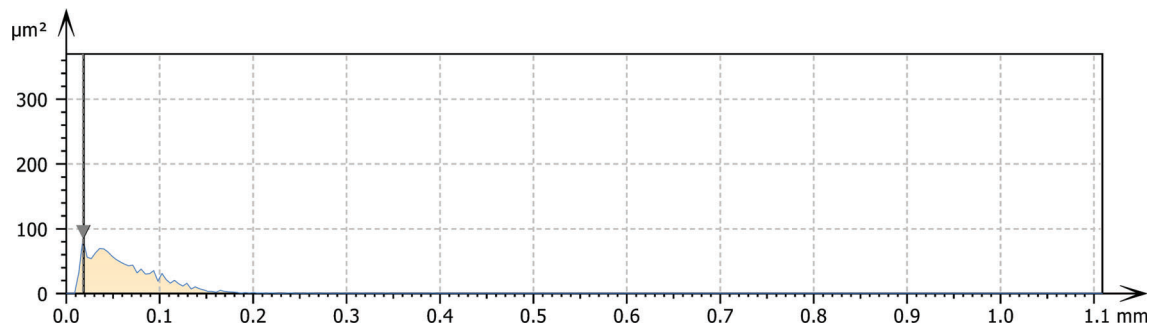
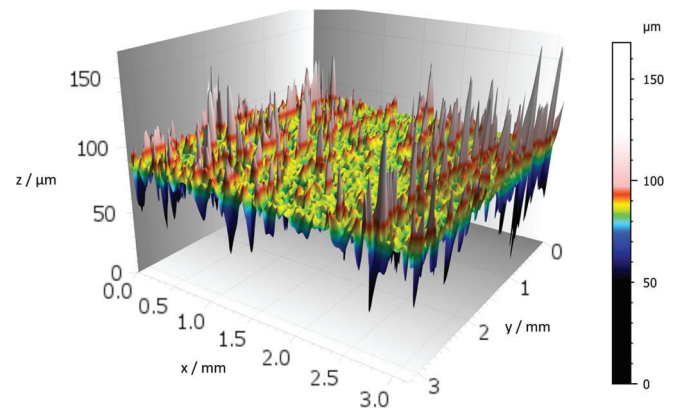


FIGURE 12 Power spectrum density of the interpolation error of the Kriging interpolation

TABLE 3 The 2.5% quantile and 97.5% quantiles of the surface texture parameters distribution, evaluated on the Kriging-interpolated surfaces obtained evaluated through the 1000 random independent samples

Parameter	S_a (μm)	S_q (μm)	S_z (μm)	S_{al} (mm)	S_{tr} (%)	S_{td} ($^\circ$)
2.5% quantile	35.2	44.4	258.3	0.143	9.5	177.0
97.5% quantile	36.2	45.8	397.4	0.154	11.2	180.0

Note: Computations have been carried out according to ISO 25178-2:2012 by means of the dedicated software MountainsMap.

The procedure has been repeated 1000 times, to provide statistical meaningfulness to the performed comparison. Each time, a random sample was extracted, the Kriging prediction was repeated and, for each prediction, the parameters characterizing the predicted surface topography were computed. In Table 3, there are the 2.5% and the 97.5% quantiles of the empirical distribution of the parameters. The reference characterization values of Table 1 are included in the confidence intervals of Table 3, concluding that the differences between the reference characterization values and the ones based on Kriging predictions (in Table 2 and formerly discussed) may be considered as not systematic.

5 | CONCLUSIONS AND FINAL REMARKS

The issue addressed in this article is the surface topography form measurement and verification. The standards provide several indices in order to detect possible technological errors and signatures in the parts. In this work, we adopted the ordinary Kriging model, which proved to be effective in predicting geometrical errors in manufacturing, and the variograms for modeling a possible correlation between the sampled points of the measured surface, according to geostatistic practices for very noisy data. The comparison between the Standard measurement approach and the Kriging methods was based both on theoretical insights about the use of the variogram in case of random sampling and on a case study based on real measurements where random sampling and Kriging predictions are used. The Kriging methodology

proved effective in predicting surface textured patterns, even if it was based on a set of sparse economic measurements. The result of Kriging interpolation, once characterized according to the Standard procedure, yielded information consistent with denser and more expensive measurement approaches. The current challenges of Industry 4.0 for surface texture characterization, hereby including freeform surfaces and additive surface, require an extremely long time, and hence high costs, to achieve an adequate and representative measurement by means of traditional devices. The SMEs would have to purchase extremely expensive new equipment (typically optical instruments) or to invest a consistent amount of time for quality assessments using the traditional one, to cope with technological challenges enforced by the current industrial framework. Thus, the adoption of the empirical variogram in detecting correlation structure as well as Kriging prediction can be considered adequate tools to achieve informativeness from sparse and cheap set of measurements statistically. Moreover, we consider our finding as an encouraging preliminary step to be used as a guide for further developments in detecting anomalies, obtaining definitive practical advantages for SMEs. Future work shall address the application of these tools for process control. A typical scenario may be the application of Kriging method for in-line process control with contact probes based on control limits set on the basis of reference surface topography measurements performed by optical devices. The software implementing the Kriging prediction can be straightforwardly incorporated into the CMM computer control, and it can run in real time; being the automation of the Kriging predictions quite inexpensive, it is possible to predict the surface texture over a tight grid, also providing a quantification of the uncertainty on the basis of the MSPE.

ACKNOWLEDGMENTS

Giovanni Pistone gratefully acknowledges the support of de Castro Statistics and Collegio Carlo Alberto. He is a member of INdAM-GNAMPA and of Enbis. Giacomo Maculotti would like to thank the support from “Ministero dell’Istruzione, dell’Università e della Ricerca” Award “TESUN-83486178370409 finanziamento dipartimenti di eccellenza CAP. 1694 TIT. 232 ART. 6.” Computational resources provided by HPC@POLITO (<http://www.hpc.polito.it>).

ORCID

Grazia Vicario  <https://orcid.org/0000-0001-9530-9673>

REFERENCES

- Schlesinger G. Research on surface finish. *J Inst Product Eng.* 1942;21(1):1.
- Whitehouse DJ. Typology of manufactured surfaces. *Ann CIRP.* 1971;19:417-431.
- Leach RK. *Characterisation of Areal Surface Texture.* Berlin, Germany: Springer; 2013.
- Chetwynd DG, McKee FA, Rakels JH. Machined surfaces: final texture and underlying structure. *Wear.* 1982;83:233-240.
- Eppinger SD, Huber CD, Pham VH. A methodology for manufacturing process signature analysis. *J Manufact Syst.* 1995;14:20-34.
- Whitehouse DJ. Surfaces – a link between manufacture and function. *Proc Inst Mech Eng.* 1978;192:179-188.
- Evans Chris J, Bryan James B. ‘Structured’, ‘textured’ or ‘engineered’ surfaces. *CIRP Ann Manufact Technol.* 1999;48:541-556.
- Aggarwal J, Kotlicki A, Mossman M, Whitehead L. Liquid transport based on electrostatic deformation of fluid interfaces. *J Appl Phys.* 2006;99(10):104904.
- El Zaatari S, Marei M, Li W, Usman Z. Cobot programming for collaborative industrial tasks: an overview. *Robot Autonom Syst.* 2019;116:162-180.
- Grabon W, Pawlus P, Wos S, Koszela W, Wiczorowski M. Effects of honed cylinder liner surface texture on tribological properties of piston ring-liner assembly in short time tests. *Tribol Int.* 2017;113:137-148.
- Etsion I, Sher E. Improving fuel efficiency with laser surface textured piston rings. *Tribol Int.* 2009;42:542-547.
- Yin Y, Stecke KE, Li D. The evolution of production systems from industry 2.0 through industry 4.0. *Int J Product Res.* 2018;56:848-861.
- Salkin C, Oner M, Ustundag A, Cevikcan E. A conceptual framework for industry 4.0. *Industry 4.0: Managing the Digital Transformation.* Cham, Switzerland: Springer; 2018:3-23.
- Jose R, Ramakrishna S. Materials 4.0: materials big data enabled materials discovery. *Appl Mater Today.* 2018;10:127-132.
- Leach RK. *Optical Measurement of Surface Topography.* Berlin, Germany: Springer; 2011.
- Leach RK, Giusca CL, Haitjema H, Evans C, Jiang X. Calibration and verification of areal surface texture measuring instruments. *CIRP Ann Manuf Technol.* 2015;64:797-813.
- Takamasu K. Present problems in coordinate metrology for nano and micro scale measurements. *J Metrol Soc India.* 2011;26:3-14.
- Gunasekaran A, Subramanian N, Ngai WTE. Quality management in the 21st century enterprises: research pathway towards Industry 4.0. *Int J Product Econom.* 2019;207:125-129.
- Savio E, De Chiffre L, Schmitt R. Metrology of freeform shaped parts. *CIRP Ann Manuf Technol.* 2007;56:810-835.
- Leach RK. Metrology for additive manufacturing. *Meas Control.* 2016;49:132-135.
- Townsend A, Senin N, Blunt L, Leach RK, Taylor JS. Surface texture metrology for additive manufacturing: a review. *Precis Eng.* 2016;46:34-47.

22. Bewilogua K, Bräuer G, Dietz A, et al. Surface technology for automotive engineering. *CIRP Ann Manuf Technol.* 2009;58:608-627.
23. Mohanty AK, Vivekanandhan S, Pin JM, Misra M. Composites from renewable and sustainable resources: challenges and innovations. *Science.* 2018;362:536-542.
24. Choi GM, Jin J, Shin D, et al. Flexible hard coating: glass-like wear resistant, yet plastic-like compliant, transparent protective coating for foldable displays. *Adv Mater.* 2017;29:1-7.
25. Pedone P, Vicario G, Romano D. Kriging-based sequential inspection plans for coordinate measuring machines. *Appl Stoch Models Bus Ind.* 2009;25:133-149.
26. Vicario G, Ruffa S, Panciani GD, Ricci F, Barbato G. Form tolerance verification using the Kriging method. *Statistica Applicata.* 2011;22:323-340.
27. Pistone G, Vicario G. Kriging prediction from a circular grid: application to wafer diffusion. *Appl Stoch Models Bus Ind.* 2013;29:350-361.
28. Ruffa S, Panciani GD, Ricci F, Vicario G. Assessing measurement uncertainty in CMM measurements: comparison of different approaches. *Int J Metrol Qual Eng.* 2013;4:163-168.
29. Ascione R, Moroni G, Petró S, Romano D. Adaptive inspection in coordinate metrology based on kriging models. *Precis Eng.* 2013;37:44-60.
30. Kolios A, Salonitis K. Surrogate modelling for reliability assessment of cutting tools. Paper presented at: Proceedings of the 11th International Conference on Manufacturing Research. Cranfield, UK. 2013:405-410.
31. Song S, Wang A, Huang Q, Tsung F. Shape deviation modeling for fused deposition modeling processes. Paper presented at: Proceedings of the IEEE International Conference on Automation Science and Engineering. Taipei, Taiwan. 2014:758-763.
32. Wang A, Song S, Huang Q, Tsung F. In-plane shape-deviation modeling and compensation for fused deposition modeling processes. *IEEE Trans Automat Sci Eng.* 2017;14:968-976.
33. Xie K, Camelio JA, Izquierdo LE. Part-by-part dimensional error compensation in compliant sheet metal assembly processes. *J Manuf Syst.* 2012;31:152-161.
34. Yue X, Shi J. Surrogate model-based optimal feed-forward control for dimensional-variation reduction in composite parts' assembly processes. *J Qual Technol.* 2018;50:279-289.
35. Cressie NAC. *Statistics for spatial data. Wiley Series in Probability and Mathematical Statistics: Applied Probability and Statistics. Revised reprint of the 1991 edition.* Hoboken, NJ: John Wiley & Sons Inc. A Wiley-Interscience Publication; 1993.
36. Pistone G, Vicario G. A note on semivariogram. In: Di Battista T, Moreno E, Racugno W, eds. *Topics on Methodological and Applied Statistical Inference.* New York, NY: Springer; 2016:181-190.
37. Pistone G, Vicario G. How to model the covariance structure in a spatial framework: variogram or correlation function? In: Makrides A, Karagrigoriou A, Skiadas CH, eds. *Data Analysis and Applications.* Vol 10. Hoboken, NJ: John Wiley & Sons, Ltd; 2020:167-183.
38. Ruffa S, Vicario G, Pistone G. Analysis of the covariance structure in manufactured parts. *Commun Stat Theory Methods.* 2015;44:4540-4551.
39. Vicario G, Craparotta G, Pistone G. Meta-models in computer experiments: kriging versus artificial neural networks. *Qual Reliab Eng Int.* 2016;32:2055-2065.
40. Vicario G, Giraud MT, Calí V. Kriging modelization in predicting metal sheet elongation. *Qual Reliab Eng Int.* 2018;34:1390-1399.
41. Vicario G, Pistone G. Simulated variogram-based error inspection of manufactured parts. *Stat Pap.* 2018;59:1411-1423.
42. Maculotti G, Feng X, Galetto M, Leach R. Noise evaluation of a point autofocus surface topography measuring instrument. *Measur Sci Technol.* 2018;29:065008-065016.
43. Maculotti G, Feng X, Su R, Galetto M, Leach R. Residual flatness and scale calibration for a point autofocus surface topography measuring instrument. *Measur Sci Technol.* 2019;30:075005-075020.
44. ISO 25178 geometrical product specifications (GPS) - surface texture: areal; 2010.
45. ISO 25178-2:2012 Geometrical product specifications (GPS) - surface texture: areal. Part 2: terms, definitions and surface texture parameters; 2012.
46. Yitzhaki S, Schechtman E. *The Gini Methodology: A Primer on a Statistical Methodology.* Springer Series in Statistics. New York, NY: Springer; 2013.
47. ISO 4287:1984 Surface roughness - terminology surface and its parameters; 1984.
48. ISO 4287:1997 geometrical product specifications (GPS) - Surface texture: profile method - Terms, definition and surface texture parameters; 1997.
49. Bruzzone AAG, Costa HL, Lonardo PM, Lucca DA. Advances in engineered surfaces for functional performance. *CIRP Ann Manuf Technol.* 2008;57:750-769.
50. Leach RK. *Fundamental Principles of Engineering Nanometrology.* Amsterdam, Netherlands: Elsevier; 2009.
51. ISO 25178-3:2012 Geometrical product specifications (GPS) - Surface texture: areal. Part 2: specification operators; 2012.
52. Cariolaro G. *Unified Signal Theory.* Berlin, Germany: Springer; 2011.
53. Santner TJ, Williams BJ, Notz WI. *The Design and Analysis of Computer Experiments.* Springer Series in Statistics. Berlin, Germany: Springer-Verlag; 2003.
54. Matheron G. Traité de géostatistique appliqué. No. 14 in Mem. Bur. Rech. Geog. Minieres Editions Technip; 1962.
55. Sacks J, Welch WJ, Mitchell TJ, Wynn HP. Design and analysis of computer experiments (with discussion). *Stat Sci.* 1989;4:409-435.
56. Sasvári Z. *Positive Definite and Definitizable Functions vol 2 of Mathematical Topics.* Berlin, Germany: Akademie Verlag; 1994.
57. Gneiting T, Sasvári Z, Schlather M. Analogies and correspondences between variograms and covariance functions. *Adv Appl Probab.* 2001;33:617-630.

58. Stehlik M, Helperstorfer C, Hermann P, et al. Financial and risk modelling with semicontinuous covariances. *Inf Sci.* 2017;394-395:246-272.
59. Schmidt M, Merklein M, Bourell D, et al. Laser based additive manufacturing in industry and academia. *CIRP Ann Manuf Technol.* 2017;66:561-583.
60. Sacks J, Schiller SB, Welch WJ. Designs for computer experiments. *Technometrics.* 1989;31:41-47.

How to cite this article: Maculotti G, Pistone G, Vicario G. Inference on errors in industrial parts: Kriging and variogram versus geometrical product specifications standard. *Appl Stochastic Models Bus Ind.* 2021;37:839–858. <https://doi.org/10.1002/asmb.2603>